FATIGUE CRACK INITIATION STAGE IN POLYCRYSTALLINE COPPER

H. Alush, A. Bussiba and Y. Katz

Cyclic micro-crack initiation at ambient temperature in polycrystalline copper was investigated. Smooth specimens were fatigued in strain controlled tension-compression at load ratio of R= -1. The study was assisted by mechanical, dislocation structures, fine scale surface slip upset features and micro-crack initiation findings. Micro-cracks tracking was provided by replication technique. As such, the study substantiated the nature of S-N_i and ε_p-N_i behavior for initiation with implications on the crack initiation life.

INTRODUCTION

Fatigue crack initiation remains a controversial issue on both qualitative and quantitative levels. Nevertheless, the micro-crack nucleation event, is a central issue in fatigue failure. Fatigue might follow nucleation or propagation controlled processes. Thus, in elastic-plastic solids, better understanding of fatigue initiation life is essential. There are at least two major fundamental approaches to fatigue crack initiation. First, the micro-geometrical model (1) that is centered on how external surface features (like slip-upset) might provide an appropriate measure for cyclic damage. Second, the energetical model (2-3) which refers to the local intensified strain sites, with dislocation structure origins (for example, persistent slip bands - PSB). As already been established (4), micro-plasticity is mainly manifested by low energy dislocation structures, which are developed during the fatigue process. Accordingly, micro-crack initiation may be controlled by surface roughening or by localized stored elastic energy, high enough to satisfy an energy criteria for micro-crack onset.

The major objective of the current paper is to provide a comprehensive experimental procedure as related to the crack initiation regime. Thus, besides searching for dislocation structures, fine scale surface features and micro-cracks tracking were done by replication technique. Such combined program allowed insights into the crack initiation life.

Nuclear Research Centre Negev, Beer-Sheva, Israel

MATERIAL AND EXPERIMENTAL PROCEDURES

Cylindrical fully hardened bars, 25 mm in diameter, of polycrystalline copper were selected. The metal purity grade (wt%) was 99.96 with impurities as specified in Table 1.

For mechanical characterization in monotonic and cyclic conditions, cylindrical specimens were utilized followed a heat treatment of 773K/3h in vacuum. The specimen geometries were according to the ASTM standards (5): 6 mm in diameter and 25 mm in gage length. For fatigue specimens, a limited area of about 10 mm in length was polished mechanically and electrolytically, to allow fine scale surface feature observations. All mechanical tests were conducted at 296K on computerized servo-hydraulic machine. The applied $\Delta\varepsilon_T$ was between 10^{-4} to 10^{-3} in strain controlled tension-compression with load ratio of R= -1. Dislocation structures were observed by Transmission Electron Microscopy (TEM) and micro-cracking detection was performed by replication technique followed by optical and Scanning Electron Microscopy (SEM) examinations. Fine surface feature findings were detected by Atomic Force Microscopy (AFM) study indicating slip-upset topography. AFM enabled to explore the local microscopic shear strain in terms of slip band height and density on almost an atomic scale.

EXPERIMENTAL RESULTS

The aforementioned annealing heat treatment resulted in grain size between 50 to 100μm with visible low annealing twins and dislocation density. Mechanical properties consisted in 35 MPa yield stress (σ_{ys}) of 0.2% off-set and ultimate stress (σ_{UTS}) of 215 MPa. The elongation and strain hardening coefficient (n) values were 55% and 0.29 respectively. More about the cyclic behavior is given in Table 2. Typical mechanical response in fatigue in terms of the stress values is shown in Fig. 1. The maximum stress vs. cumulative cyclic plastic strain (ε_{cmu}) up to ε_{cmu} of 100% is given in Fig. 2. For the sake of completeness, the monotonic behavior is depicted as well.

TABLE 1 - Impurities content in ppm.

Al	Co Zr V Ba Fe Mo Ca Mg	Cd Cr Ni Zn	Sr Mn
100	in the order of 10	in the order of 5	less than 2

TABLE 2 - Some features in cyclic behavior.

	$\frac{\Delta\varepsilon_T}{2}$	$\frac{\Delta\varepsilon_P}{2}$	σ_{ys} (MPa)	n	$\sigma_{saturation}$ (MPa)	Initiation cycles N_i^*	Saturation cycles N_s
Monotonic			35	0.29			
Cyclic	$6\,10^{-4}$	$1\,10^{-4}$	25	0.16	60	700-1000	2500
Cyclic	$8\,10^{-4}$	$2\,10^{-4}$	30	0.15	76	400-600	1000
Cyclic	$1.5\,10^{-3}$	$7\,10^{-4}$	37	0.13	107	100-200	400
Cyclic	$2.2\,10^{-3}$	$1.2\,10^{-3}$	47	0.25	116	0-100	200

* determined by using the replica technique tracking.

Micro-crack detection by replication followed by SEM observations enabled to track early stages of crack formation. As given in Fig. 3, crack size distribution is clearly observed beside the enhanced tendency for coalescence and growth. At this early stage, isolated cracks approached a microscopical crack size. Dislocation structures developed as observed in fatigue at low strain amplitudes indicated high dislocation density, which were followed at early stages by localization beside dislocation-free zones. Typical sequence corresponded to structures as loop patch, veins of loop patch (see Fig.4), veins and ladder in PSB. In high plastic strain amplitudes, dislocation structures resembled the types formed by monotonic loading, namely elongated cells labyrinth and more of symmetrical cell structures. Generally, in monotonic and cyclic loading, vein separation distance and the cell size were strain amplitudes dependent.

As observed, the vein distance and the cell size decreased as the plastic strain amplitude increased. Insights regarding the low energy dislocation structures are revealed by TEM observations as indicated in Tables 3 and 4. Crack initiation tracking by replication technique (see Table 2) up to the coalescence of micro-crack clusters revealed that micro-cracks formed mainly at PSB. However, the issue of surface roughness as cracking origins or sites for enhanced PSB formation was also examined. In this context of slip-upset, some findings promoted by AFM are shown in Table 5. Fig. 5 illustrates a typical example of AFM features in case of cyclic loading. Notice that the AFM enabled quantitative measurements of the localized shear strain, which appears to be an appropriate measure of fatigue damage.

At this stage, it became apparent that localized damage intensified with strain amplitude increase. Thus, not only the ratio between the displacement height and the slip spacing was considered but also the fatigue efficiency factor. The study revealed surface roughness increase for higher normal strain amplitude values beside higher fatigue efficiency factor for surface damage, which was history dependent (decrease with the number of cycles).

TABLE 3 - Cells size measures.

Loading form	Strain (%)	Stress (MPa)	Average of cells size (μm)
monotonic tension	6	127	1.06±0.34
monotonic tension	22	204	0.807±0.12
monotonic tension	55	Fracture	0.392±0.1
cyclic loading $\Delta\varepsilon_T/2=2.2\cdot10^{-3}$	2400	116	1.6±0.38

TABLE 4 - Vein distance measures.

Total strain amplitude	Veins distance (μm)
$6\cdot10^{-4}$	1.66±0.104
$8\cdot10^{-4}$	0.92±0.05
$1.5\cdot10^{-3}$	0.5±0.021

TABLE 5 - Fine scale features provided by AFM (average value of 5 measurements).

Test condition	$\Delta\varepsilon_p/2$	Surface features	Slip spacing (nm)	Slip height (nm)
No loads	---	Smooth	Surface roughness of 0.5	
Cyclic	$8\cdot10^{-4}$	Inhomogeneous - slip upset	45	15
Cyclic	$1.5\cdot10^{-3}$	Inhomogeneous - slip upset	48	25

DISCUSSION

Crack initiation behavior and life, was basically assisted by a model and simulation study which provided S-N_i curves or Manson-Coffin relationship for crack initiation only. The pattern of this formulation is now briefly described. Based on the well-respected Cottrell model, the total energy U for a loaded cracked segment is given by (6);

$$U = \frac{\mu n^2 \bar{b}^2}{4\pi(1-\upsilon)} \ln\left(\frac{4R}{\alpha}\right) + 2\gamma a - \frac{8n\bar{b}a}{2} - \frac{\pi(1-\upsilon)S^2a^2}{8\mu} \qquad (1)$$

if $a = n\bar{b}$ and instability occurred due to critical number of dislocation prior to pile-up collapse, the number of cycles for initiation may be described by a condensed form;

$$N_i = \frac{\ln \psi(A,B,C)}{\lambda X} \qquad (2)$$

where: $A = n\bar{b}/8\pi(1-\upsilon)\gamma$; $B = \bar{b}/4\gamma$; $C = \pi(-\upsilon)\bar{b}/8\mu\gamma$

This formulation with appropriate modification regarding influence of the friction stress and the fatigue efficiency factor allowed establishing S-N_i dependency and ε_p-N_i relationship. Here, the simulation analyzed the role of several critical variables on crack initiation, (including damage efficiency, surface energy, grain size and the friction stress). Moreover, the proposed model resulted in a Manson-Coffin damage rule for initiation, which predicted steeper slops for initiation.

$$\Delta\varepsilon_p/2 = A(2N_i)^{-1} \qquad (3)$$

Here micro-cracking formation occurred in the range of cumulative plastic strain in the specific range between 0.4 to 0.6. Thus for this case: $\Delta\varepsilon_p/2=0.4\text{-}0.6(2N_i)^{-1}$. Experimentally (see Fig. 6), a slop of –0.84 (approaching –1) was confirmed in contrast to about –0.5 normally obtained for fatigue failure's life.

It appears that kind of fatigue damage rules for crack initiation that either S-N_i or ε_p-N_i are appropriate. Since crack initiation occurred prior to stress stabilization, microstructural origins (grain boundaries or twinning) beside purity effects were hypothesized. Thus, in order to conduct an appropriate evaluation of the experimental findings, the fatigue damage effectiveness and friction stress functions became essential. Along those modifications, cumulative damage formulation was attempted which turned out to be consistent with both the geometrical and the energetical models. It became also

apparent that the initiation life is highly dependent on the plastic amplitude values (more than in the failure life) indicating that crack shielding effects are more retarded in the initiation regime. Generally, the study extended the definition of crack initiation by realizing subsequences from initial precrack events, crack formation (localized), micro-cracks clusters (global behavior) up to micro-crack coalescence or elongated crack (again in highly localized sense). Note that the early stage of initiation was associated with limited number of cycles (this has been confirmed also by fatigue torsional tests). However, the present definition of small cracks is not under the category of micro-structural crack size.

Finally, the potential of novel techniques in exploring fundamental and critical issues as related to fatigue damage are described and further assessed.

CONCLUSIONS

(1) Plastic amplitude is the dominant variable in the crack initiation life with threshold wise behavior.
(2) The role of the fatigue efficiency damage factor on crack initiation is critical.
(3) Crack initiation can be formulated by basic laws of damage accumulation, which remain consistent with the micro-energetical and the micro-geometrical models.
(4) Low cycle fatigue approach assists in elucidating the complex crack initiation regime.

ACKNOWLEDGMENTS

The authors appreciate the assistance by Dr. E. Grossman from the NRC – Soreq and by Messrs E. Woodbeker, R. Shefi, A. Sobel and M. Kupiec from NRC – Negev, Israel.

SYMBOLS USED

a	= length of extending crack
$\bar{b}$	= Burger`s vector
n	= number of dislocations
R	= effective radii of dislocations domain for crack initiation
S	= supplied stress range
X	= dislocation pile-up length
$\gamma, \lambda, \upsilon$	= surface energy, combined material constant and poisson ratio
$\Delta\varepsilon_T, \Delta\varepsilon_P$	= total and plastic strain range

REFERENCES

1. Harvey, S. E., Marsh, P. G. and Gerberich, W. W., Acta Metall. Mater., Vol. 42, No. 10, 1994, pp. 3493-3502.
2. Tanaka, K. and Mura, P., J. App. Mech, Vol. 48, 1990, pp.97-102.
3. Mura,T. and Nakasone, Y., J. App. Mech., Vol. 57, 1990, pp. 1-6.
4. Lin, M.R., Fine, M.E. and Mura,T., Acta Metall., Vol. 34, No. 4, 1986, pp. 619-628.
5. ASTM Standard E606-92, 1997, pp. 523-537.
6. Cottrell, A.H., Trans. of the AIME, Vol. 212, 1958, pp. 192-202.

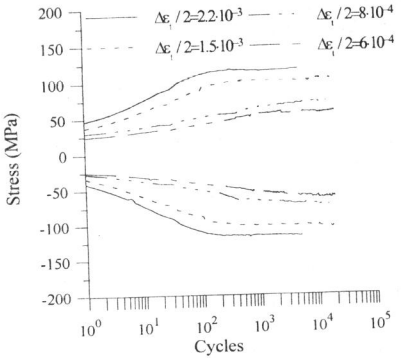

Figure 1 Fatigue stress values vs. cycles for various strain amplitudes.

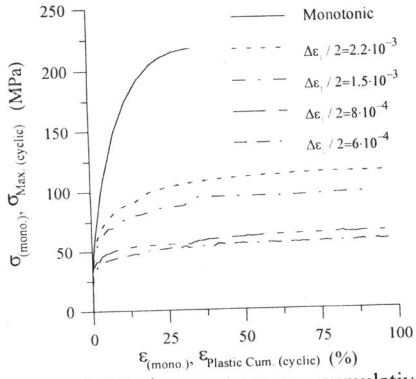

Figure 2 Maximum stress vs. cumulative cyclic plastic strain up to 100%.

Figure 3 Micro-crack of 15μm followed PSB after 1000 cycles for $\Delta\varepsilon_T/2 = 8 \cdot 10^{-4}$.

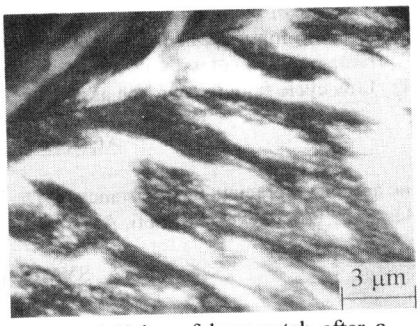

Figure 4 Veins of loop patch after ε_{cum} = 800% with $\Delta\varepsilon_T/2 = 6 \cdot 10^{-4}$.

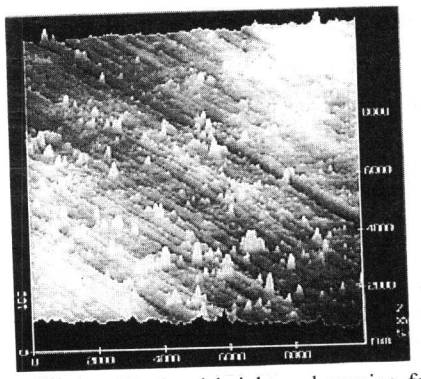

Figure 5 Slip band height and spacing for 10^4 cycles observed by AFM (3D display).

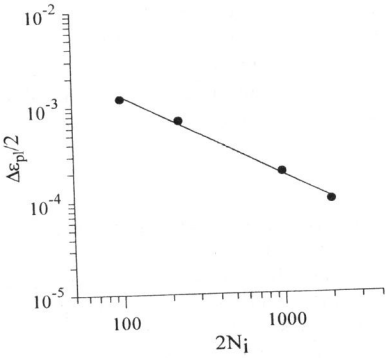

Figure 6 Plastic strain amplitude vs. crack initiation cycles.